JOURNAL OF SOLID STATE CHEMISTRY 99, 303–312 (1992)

Synthesis of High Surface Area Vanadium Nitride

RAJAT KAPOOR* AND S. TED OYAMA†,*,[1]

*Departments of *Chemical Engineering and †Chemistry, Clarkson University, Potsdam, New York 13699-5705*

Received September 30, 1991; in revised form February 7, 1992; accepted February 12, 1992

Fine vanadium nitride powders (particle size 11 nm) have been prepared by temperature programmed reduction and nitridation of V_2O_5 by gaseous ammonia. The reaction was followed by monitoring gas phase reaction products by on-line mass spectroscopy. X-ray diffraction and elemental analysis were used to identify various solid-state reaction intermediates, V_6O_{13}, V_2O_4, VO_2, V_2O_3, and VO, and to establish that the final reaction step was the nitridation of VO to VN. Heating rate had a substantial effect on product specific surface area and a rate of 0.083 K sec^{-1} resulted in an optimal value of 90 m^2g^{-1}. The activation energy for nitridation was not constant, but rose from 203 to 243 kJ mol^{-1} as the extent of reaction increased from 0.25 to 0.75. The transformation was limited by the bulk diffusion of oxygen and nitrogen and not by a surface process.

Introduction

Transition metal carbides and nitrides combine extreme hardness and strength with high melting points (*1*). Their applications are varied, ranging from cutting tools and structural materials (*2, 3*) to magnetic and electronic components (*4, 5*), superconductive devices (*6–8*), and catalysts (*9–11*). For processing of advanced ceramics the particle size of the starting powder is an important parameter (*7, 12*). Small particle sizes provide ductility through differential creep mechanisms (*13, 14*) and allow for greater densification because of the dependence of sintering on the inverse fourth power of particle size (*15*). Because of this, interest in synthesis of high surface area materials has grown in recent years.

In the field of catalysis carbides and nitrides have attracted attention because of advantages in activity, stability, selectivity, and resistance to poisoning over the parent transition element (*10, 16–18*). The catalytic behavior of the compounds resembles those of the noble Group VIII metals (Pt, Pd, Rh, etc.), (*9, 10, 16*), thus offering an economical substitute for these rare and expensive metals. For effective use, a substantial exposure of the catalytic material to the reactive medium is required, and therefore, it is important to have high specific surface area, S_g.

Significant progress towards preparation of these materials with high S_g was made with a temperature-programmed method of synthesis (*19*). A lot of work has been done in the synthesis and characterization of these compounds, with focus on Mo_2C (*17, 20–23, 30*), Mo_2N (*21, 24, 30*), and WC (*20, 30*).

[1] To whom correspondence should be addressed.

0022-4596/92 $5.00

This paper deals with the synthesis of VN. Vanadium nitride exists in two crystalline forms, δ-VN (B1 cubic) and β-V_2N (hcp), over a wide range spanning $VN_{1.000}$–$VN_{0.155}$ (*25*). Conventional isothermal preparation of δ-VN involves heating NH_4VO_3 in flowing dry NH_3 at 1373 K (*26*), to produce a nitride of low S_g, 0.32 $m^2\ g^{-1}$ (*27, 28*).

We have prepared high S_g (90 $m^2\ g^{-1}$) δ-VN powders by temperature-programmed reaction (TPR), a technique in which a V_2O_5 precursor is reduced and nitrided by reaction with NH_3 gas, while the temperature is progressively raised (*19*). Initial results with the TPR method produced a VN of 38 $m^2\ g^{-1}$ (*29*). This paper investigates the solid-state transformation of V_2O_5 to VN by following the progress of synthesis by on-line mass-spectrometry. X-ray diffraction (XRD) and gas adsorption techniques are used to characterize the intermediates and products.

Experimental

The gases employed in this study were NH_3 (Linde Anhydrous Grade, 99.99%), He (Linde UHP Grade, 99.999%), 0.5% O_2/He (Linde UHP Grade), 20% CH_4/H_2 (Linde UHP Grade), and H_2 (Linde UHP Grade, 99.999%). The chemicals used were V_2O_5 (Aesar, 99.9%) and MoO_3 (Aldrich, 99.5%). The chemicals used for analytical reference were V_6O_{13} (Alfa, 99.5%), VO_2 (Alfa, 99%), V_2O_4 (Alfa), V_2O_3 (Alfa), VO (Alfa, 99.5%), VN (Alfa 99.5%), and V (Alfa, 99.5%). All reagents were used as received.

The reactor consisted of a quartz U-tube of 15-mm O.D. placed in a furnace (Hoskins, 550 W) controlled by a temperature programmer (Omega Model CN2000). The temperature of the sample was measured with a chromel–alumel thermocouple placed in a well located at the center of the reactor bed. The temperature of the furnace and reactor bed, and mass spectrometer, were recorded by a computer (Thoroughbred, 80386SX-16) through and RS232 interface.

The effluent stream was leaked into a mass spectrometer (Ametek/Dycor Model MA100) chamber through a variable leak valve (Granville Phillips Model 203). The lines connecting the reactor to the analytical system were made of 1/8 in. OD stainless steel and gave rise to a negligible delay of only 0.6 sec.

The preparation procedure consisted of establishing reactant gas NH_3 flow (typically, 800 μmol sec^{-1} or 1200 $cm^3\ min^{-1}$) over the precursor V_2O_5 (400 mg, 2200 μmol) and starting the heating program. The temperature was raised in two stages, first, quickly to 430 K, and then, uniformly at a slower heating rate to the maximum temperature (T_{max}). No reactions occurred in the first heating interval. The heating rates employed in the second stage varied from 0.01 to 0.40 K sec^{-1} with T_{max} ranging between 837 and 1073 K. The total pressure was maintained at 0.17 MPa. The mass spectrometer signal and temperature were recorded in real-time, enabling determination of different stages in the synthesis.

On reaching T_{max}, the flow was switched to pure helium and the reaction was quenched by removing the reactor quickly from the furnace. After the reactor was cooled to room temperature (RT), the flow was switched to 0.5% O_2/He for passivation of the pyrophoric material. Passivation is a procedure in which low-concentration oxygen from a gas stream is chemisorbed on the surface of a material to deposit a monolayer of protective oxide.

The reactor was then transferred to another unit for characterization of the sample surface by CO chemisorption at RT and physisorption of N_2 at liquid nitrogen temperature. CO chemisorption is a technique used to titrate the number of surface metal atoms in catalysts. Pretreatment of passivated VN generally consisted of reduction of samples in 50% H_2/He at 723 K for two hours to remove the surface oxide. Finally, XRD analy-

sis was carried out using a powder diffractometer (Siemens, Model D 500 with a Cu$K\alpha$ monochromatized radiation source) operated at 40 kV and 30 mA. Nitrogen determination was by Kjeldahl analysis.

The rate of NH_3 decomposition, was measured on a sample prepared with a heating rate of 0.083 K sec^{-1} up to a T_{max} of 930 K under 0.17 MPa pressure. Rates were determined at 933 K from the increase in flow rate due to volume expansion. The inlet flow rate was 270 μmol sec^{-1} of pure NH_3. To study the effect of water vapor, the unit was modified by adding an evaporator containing distilled water to the inlet gas stream, and the synthesis again used a heating rate of 0.083 K sec^{-1}. The water vapor partial pressure was about 2 kPa.

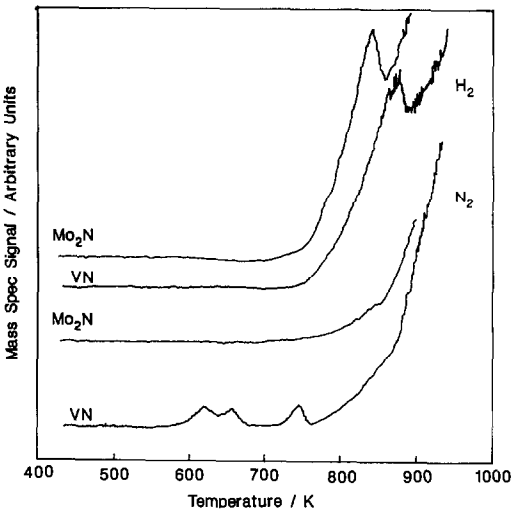

FIG. 2. Comparison of TPR of VN and Mo_2N, signal vs T.

Results

Figure 1 shows the traces of masses 2, 15, and 28 versus temperature for a TPR using 0.083 K sec^{-1} (5 K min^{-1}). The signal at mass 15 (NH), representing ammonia, gradually decreased above about 800 K. The traces of masses H_2 (2) and N_2 (28) had more features, showing a number of peaks. Separate experiments were run, interrupting the reaction after each of the N_2 and H_2 peaks at points a–f (Fig. 1). The signal at masses 2, 15, and 28 were not corrected for the relative sensitivity of H_2, NH_3, and N_2, because only changes in signal were important to follow the progress of the synthesis. However, the H_2 signal was calibrated by injecting known quantities of H_2 for determination of nitridation rates. No nitrogen oxides (NO, NO_2, N_2O) were detected even at very low concentrations. For the preparation of Mo_2N under similar conditions (Fig. 2), the mass spectrometer traces showed only the H_2 peak, with the N_2 peaks being absent.

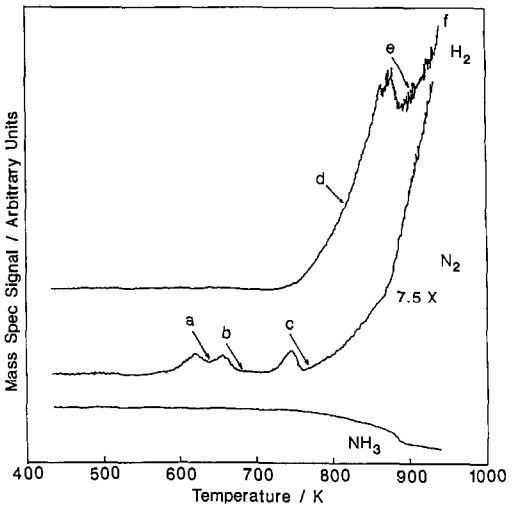

FIG. 1. Mass spectrometer signal for temperature-programmed reaction of V_2O_5, signal vs T.

XRD analysis (Figs. 3–5) of the products obtained after stopping the reaction at different stages (a–f) showed the transformation of the V_2O_5 starting material to various suboxide intermediates. The XRD pattern of standards have been appropriately interspersed among the experimental ones for comparison.

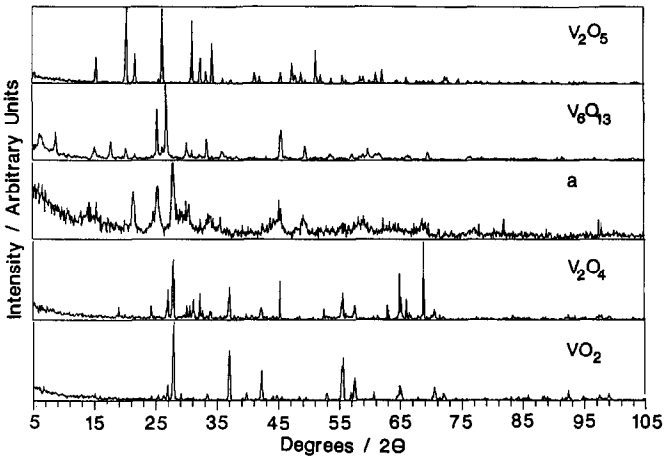

FIG. 3. XRD patterns of samples and standards: Early stages, intensity vs 2θ.

The BET specific surface area (S_g) of the intermediates (Fig. 6) developed during synthesis, starting at 19 $m^2\ g^{-1}$ for V_2O_5 and increasing up to point e, after which they leveled out to approximately 90 $m^2\ g^{-1}$. S_g increased with heating rate up to a maximum of 90 $m^2\ g^{-1}$ at 0.083 K sec^{-1}, beyond which it fell to 60 $m^2\ g^{-1}$ and remained constant (Fig. 7). Many of the experiments reported in this paper were carried out with the 0.083 K sec^{-1} heating rate because of the optima S_g produced.

In the experiment for the study of the effect of water vapor on the synthesis, it was found that the three N_2 and one H_2 peaks a 610, 640, 720, and 880 K were shifted to higher temperatures, 618, 718, 922, and 98 K, respectively, upon addition of water. S_g was determined to be 38 $m^2\ g^{-1}$, which was considerably smaller than the 90 $m^2\ g^{-1}$ ob

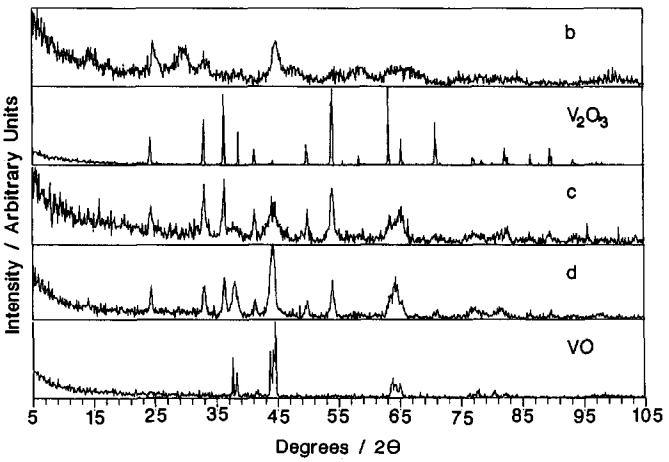

FIG. 4. XRD patterns of samples and standards: Intermediate stages, intensity vs 2θ.

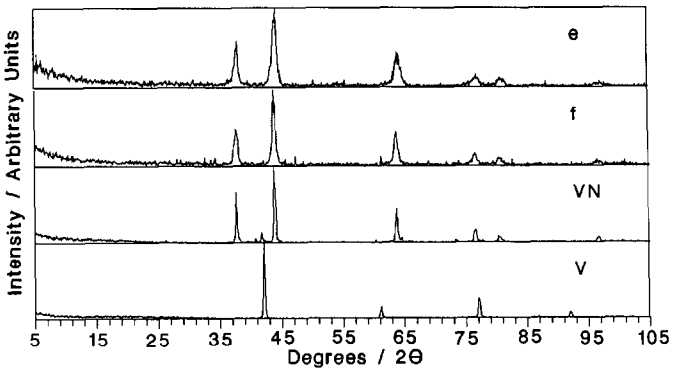

FIG. 5. XRD patterns of samples and standards: Final stages, intensity vs 2θ.

tained without the water. The reduction of V_2O_5 was studied with a 3 : 1 H_2/He stream at the standard heating rate of 0.083 K sec^{-1}. The final product was found to be V_2O_3 at T_{max} as high as 1313 K.

Discussion

TPR involves the conversion of an oxide precursor to a carbide or nitride in a flowing reactive gas stream, followed by mass spectrometry. In the past, reaction products have been detected by gas chromatography (*17*) or by on-line thermal conductivity (TC), (*19*). Although TC signals have been useful for following the progress of carbide preparations, for nitrides the signal is overwhelmed by the NH_3 decomposition reaction (*30*).

In contrast, mass spectrometry gives precise indications of the occurrence of sequential solid-state transformations (Fig. 1). The figure shows changes in the signals for masses 2, 15, and 28 as the temperature of the sample is raised. Mass 15 (NH_3) drops in intensity at around 800 K due to the decomposition of ammonia. Masses 2 and 28 provide substantially more information. At relatively low temperatures three positive N_2 (28) peaks occur without any accompanying H_2 (2) peaks. This suggests that the hydrogen produced by the decomposition of NH_3 is being consumed in some reductive process. Indeed, the XRD patterns of the intermediates obtained by interrupting the reaction in separate runs (labeled a–c in Fig. 1) show the presence of various reduced species. There are no accompanying changes in the NH_3 signal because its concentration is orders of magnitude larger than the N_2 and H_2 levels and its consumption is low. Mass 18 (H_2O), not shown, is affected by the very large signal at mass 17 (parent NH_3 ion) and lacks sufficient sensitivity to show reduction peaks.

In the high temperature region where there

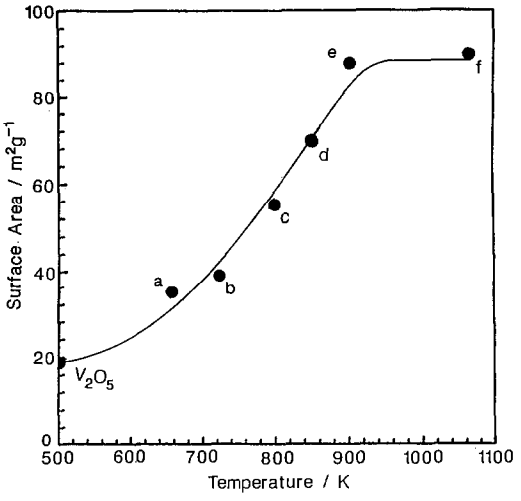

FIG. 6. Development of surface area during synthesis, S_g vs T.

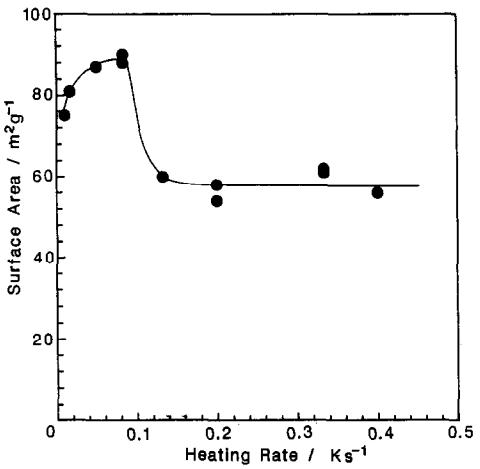

FIG. 7. Effect of heating rate on surface area, S_g vs β.

is substantial ammonia decomposition, a peak in the H_2 signal is observed but not in the N_2 signal. The hydrogen peak probably appears because some of the H_2 from NH_3 is desorbed at the time N is being consumed in the nitridation process. Another possibility is that the change in H_2 signal is not a peak, but a dip that marks the formation of a bulk hydride. Hydrides are common among early transition metals (*31–34*). However, XRD patterns and quantization of the H_2 signal suggests that hydrides are not forming.

Calibration of the hydrogen peak area allowed calculation of an average rate of nitridation per unit surface area of 1.0×10^{-5} μmol N cm^{-2} sec^{-1}. Independently, the average rate of nitridation for the transformation of VO to VN (*vide infra*), obtained from the experimental values of heating rate, surface area and number of moles, was found to be 1.2×10^{-5} μmol N cm^{-2} sec^{-1}. This good agreement strongly indicates that hydrogen is being released in the form of a peak during the final nitridation process. Alternatively, if the hydrogen signal were a dip, the resulting product formula would be approximately VH_2N, a stoichiometry too high in hydrogen.

Intermediate a (Fig. 3) obtained after the first nitrogen peak, shows substantial differences from the V_2O_5 starting material. Comparison to the V_6O_{13} and V_2O_4 standards shows that it is a mixture of the two phases. In the next stage of reduction, the pattern of intermediate b (Fig. 6) indicates that it is VO_2 (*35*), in a disordered state. The commercial VO_2 XRD pattern, shown in Fig. 5, is different from (*35*) and is seen to resemble V_2O_4. Intermediate c, obtained after the third nitrogen peak, is predominantly V_2O_3 with a small amount of VO.

The XRD pattern of intermediate d (Fig. 4) prior to the H_2 peak shows it to be predominantly VO with some unreacted V_2O_3. The V_2O_3 has experimental lattice parameters, $a_0 = 0.4945$ nm and $c_0 = 1.391$ nm, which are contracted from those of stoichiometric V_2O_3, $a_0 = 0.5105$ nm and $c_0 = 1.4449$ nm (*36*). This suggests that the V_2O_3 is slightly reduced, and that there is no nitrogen incorporation into its corundum structure, since that would result in expansion of the lattice. Although VO and VN have very similar B1 patterns, they can be distinguished by their lattice constants, 0.409 and 0.414, respectively (*37*). Sample d has a unit cell parameter of 0.4095 nm (±0.0004 nm), which corresponds to that of VO. Thus, intermediate d involves a stage of transformation in which V_2O_3 is reduced to VO.

Sample e (Fig. 5), after the hydrogen peak also has the B1 cubic pattern, but with an expanded lattice parameter of 0.411 nm, consistent with nitrogen incorporation. If further reduction of VO to a suboxide had occurred the lattice parameter would have decreased as for the case of $VO_{0.8}$ with lattice constant 0.4042 nm (*38*). Thus, an oxynitride is probably being formed. Indeed, elemental analysis of sample e indicates a nitrogen content of 14.0 wt%, compared to the theoretical maximum expected for VN of 21.4 wt%. Evidently, the mass spectrometer hydrogen peak does mark a stage of nitridation. Sample f shows the VN pattern with a lattice parame

ter of 0.413 nm and a nitrogen content of 20.2 wt%. The small discrepancy with the theoretical is probably due to remnants of oxygen in the bulk and/or the surface passivation layer, or nonstoichiometry.

Reduction with H_2 instead of NH_3 results only in the formation of V_2O_3 even at temperatures as high as 1313 K. This confirms the results by King and Sebba (*27*) who also observed no VO or V metal. NH_3 is able to carry out the further transformation of V_2O_3 because it is a stronger reducing agent than H_2. In the nitridation of V_2O_5 with ammonia (ammonium vanadate decomposition), King and Sebba (*27*) speculated that the first atoms of nitrogen reacted with V_2O_3 and entered the corundum structure to form V_2O_2N, weakening the lattice in the process. Further nitridation was thought to break up the corundum structure into a VO-VN substitutional alloy which ultimately transformed to VN. Our results are not fully consistent with this interpretation. Although we did see the final VO–VN oxynitride alloy, we found reduction to VO prior to nitridation.

Figure 2 compares the H_2 and N_2 signals obtained in the synthesis of Mo_2N from MoO_3 under similar conditions with those measured in the synthesis of VN. No peaks appeared in the N_2 trace. This suggests that the initial reduction of MoO_3 does not proceed through discrete suboxide stages as in the case of V_2O_5. Indeed, Volpe and Boudart found that the nitridation of MoO_3 proceeded by *continuous* oxynitride phases, MoO_xN_y, (*24*). This negates the results shown by Lee *et al.*, where MoO_2 is reported as an intermediate species (*23*). The discrepancy is probably due to the higher rates of reduction in the studies of Lee, *et al.*

In the course of the transformation a–f, the specific surface area (S_g) increased from 19 $m^2\ g^{-1}$ for the precursor V_2O_5 to 90 $m^2\ g^{-1}$ for the initial and final VN products e and f (Fig. 6). The CO uptake at RT of sample f was 101 μmol g^{-1} and the calculated number density of metal atoms was $6.8 \times 10^{17}\ m^{-2}$. This was low compared to the expected value of $10^{19}\ m^{-2}$, and could be due to the presence of adsorbed oxygen or nitrogen atoms.

TABLE I

CALCULATED PARTICLE SIZES

Species		Density (g cm^{-3}) ρ	Particle size (nm) D_p	Crystallite size (nm) D_c
Starting material	V_2O_5	3.4	94	83
Intermediate c	V_2O_3	5.0	22	19
Intermediate e	"VO"	5.8	11	12
Product f	VN	6.1	11	14

Crystallite sizes averaged over low index planes were estimated with the Scherrer equation, $D_c = K\lambda/\beta \cos\theta$, where λ is the wavelength of the X-ray radiation, 0.154 nm, θ the Bragg angle, and β the width of the XRD peak at half-maximum corrected for instrumental broadening (0.1°), and K is a constant taken to be 0.9 (*39*). For the transformation $V_2O_5 \rightarrow$ VN, D_c decreased from 83 to 14 nm. Corresponding particle sizes were calculated from the equation (*40*), $D_p = 6/(S_g\rho)$, where ρ is the density of the solid (Table I). The good agreement between D_p and D_c indicates that the particles are not polycrystalline.

Effect of water vapor. It was found that water vapor in the reactant stream, decreased S_g of the product from 90 to 38 $m^2\ g^{-1}$. This supports the studies of Oyama *et al.*, based on space velocity variation measurements, which concluded that H_2O was responsible for low S_g (*30*). In the present studies the three N_2 peaks and the H_2 peak shifted to higher temperatures in the presence of H_2O. This suggests that H_2O does not cause hydrothermal sintering by migration of mobile hydrated species (*41*), but retards the synthesis process by inhibiting reduction. Thus for the same extent of reaction, higher temperatures than usual are required.

Calculation of activation energy, E_a. The H_2 peak in the mass spectrometer signal has been shown to correspond to the transforma-

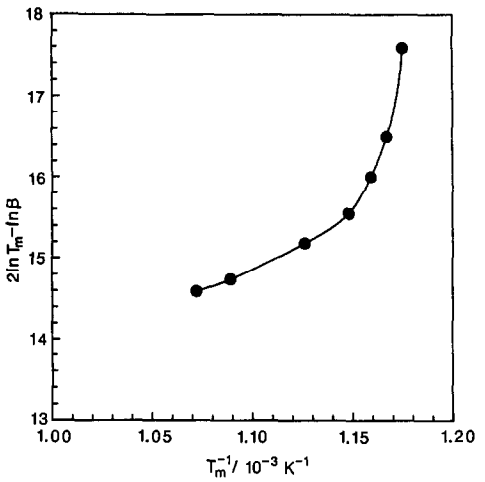

FIG. 8. Standard activation energy analysis, 2 ln T_m − ln β vs $1/T_m$.

tion of VO to VN by XRD and elemental analysis. TPR theory provides a means of calculating E_a for both surface processes such as desorption (*42–44*), and bulk processes such as reduction (*44*, *45*). In the theory, the transformation temperature corresponds to the maximum rate of reaction and, in this case, is given by the peak in the H_2 signal. TPR theory (*45*) predicts that the transformation temperature, T_m, and the heating rate, β, are related to E_a by the Redhead equation, $2 \ln T_m - \ln \beta = E_a/RT_m + \text{constant}$. A plot of $(2 \ln T_m - \ln \beta)$ vs T_m^{-1} ordinarily, gives a straight line of slope $-E_a/R$. However, the actual plot shows curvature (Fig. 8). The least-square average gives a value of 250 kJ mol^{-1} for E_a that is consistent with the reported E_a for synthesis of carbides and nitrides obtained by a simpler analysis (*30*). The value corresponds to that of diffusion of oxygen in oxides and, thus, this process was suggested to be limiting the reaction rate (*30*).

To account for the curvature, a dependence of E_a on the extent of reaction, f, was considered, $E_a = E_0 + \alpha f$. Here, α is a constant and the extent of reaction is the fraction of the final reaction, VO → VN, which occurs. The data were re-examined using line shape analysis (*46*). The true H_2 peaks were obtained by subtracting from the original signal the background, approximated by a polynomial fit (Figs. 9a,b). For each peak (different β), the extent of reaction was determined from the ratio of the area under the curve (shaded) to the total area (Fig. 9b). By taking successive areas, values of rate and temperature at increasing f could be determined for each peak (Fig. 9). Then, keeping f constant, Arrhenius plots of ln(rate) vs T^{-1} (Fig. 10) yielded values for E_a from slopes of the linear fits. E_a increased from 203 to 243 kJ mol^{-1} as the extent of reaction increased from 0.25 to 0.75.

The finding here that activation energy increases with extent of reaction is not surprising. A reason for this is that metal–oxygen bonds, in general, become stronger as an oxide is reduced because of increasing bond order. This is manifested, for example, in increased oxide melting points with extent of reduction. A more important factor is probably that the rate of transformation is determined initially by the diffusion of oxygen and later by the more difficult diffusion of nitrogen. It is known that the E_a for diffusion of nitrogen is higher than that for diffusion of oxygen (*30*).

The formation of VN is not limited by the supply of nitrogen by a surface reaction. This is confirmed by comparing the relative magnitudes of the steady-state catalytic decomposition of NH_3 on the surface and the average rate of nitridation. At 933 K, the rate of NH_3 decomposition was found to be 7.3×10^{-5} μmol cm^{-2} sec^{-1}, higher than the rate of nitridation, determined earlier to be 1.2×10^{-5} μmol cm^{-2} sec^{-1}. The apparent activation energy for the decomposition of NH_3 was also found to be 76 kJ mol^{-1}, a value that deviates

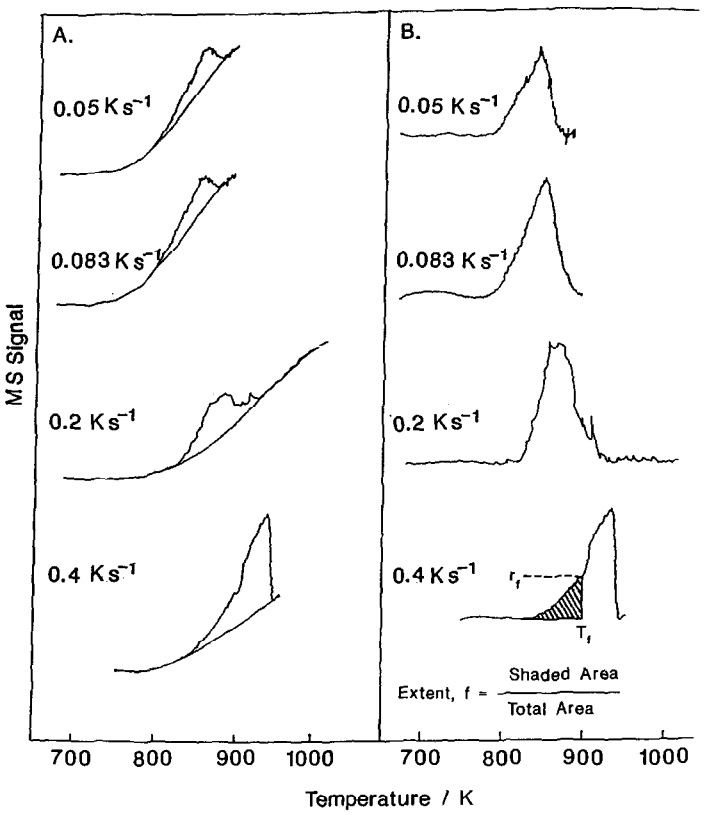

FIG. 9. Line shape analysis.

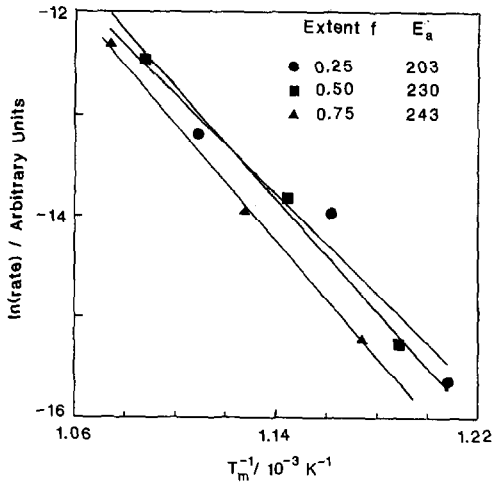

FIG. 10. Arrhenius plots for nitridation.

from that of the synthesis. Thus, as with the majority of solid state transformations (*47*) the nitridation reaction is limited by a bulk diffusion process.

Conclusions

TPR of V_2O_5 can be used to prepare high surface area (90 $m^2 g^{-1}$) VN of nanometers crystallite size. The reaction proceeds in stages, with initial reduction to various suboxide intermediates and final nitridation of VO to VN. The optimum heating rate for obtaining maximum surface area was 0.083 K sec^{-1}. Water vapor in the feed inhibited the reduction process. Line shape analysis of the TPR curves revealed that the activation energy for the nitridation reaction was

not constant but increased with extent of reaction. The transformation is probably limited initially by the bulk diffusion of oxygen and later by the diffusion of nitrogen.

Acknowledgments

This paper was written with support from the New York State Science and Technology Foundation and from the U.S. Department of Energy under the Advanced Coal Research at U.S. Universities Program, Grant DE-FG22-91PC91298.

References

1. L. E. Toth, "Transition Metal Carbides and Nitrides," Academic Press, New York (1971).
2. G. W. Wilner and J. A. Berger, *J. Met.* **7,** 360 (1955).
3. Y. M. Shy, L. E. Toth, and R. Somasundaram, *J. Appl. Phys.* **44,** 5539 (1973).
4. T. Yamada, M. Shimada, and M. Koizumi, *Ceram. Bull.* **59,** 611 (1980).
5. R. Kieffer and F. Benesovsky, "Hartstoffe," Springer-Verlag, Vienna (1963).
6. N. Pessall, R. B. Gold, and H. A. Johansen, *J. Phys. Chem. Solids* **29,** 19 (1968).
7. R. M. Powell, W. Skocpol, and M. Tinkham, *J. Appl. Phys.* **48,** 788 (1977).
8. K. Hechler and E. Saur, *Z. Phys.* **2051,** 392 (1967).
9. R. B. Levy and M. Boudart, *Science* **181,** 547 (1973).
10. S. T. Oyama and G. L. Haller, *Catalysis, Spec. Period. Rep.* **5,** 333 (1981).
11. S. T. Oyama, *Catal. Today,* **15,** 1 (1992).
12. H. Hahn, J. Logas, and R. S. Averback, *J. Mater. Sci.* **5,** 609 (1990).
13. C. Herring, *J. Appl. Phys.* **21,** 437 (1950).
14. R. L. Coble, *J. Appl. Phys.* **34,** 1679 (1963).
15. R. J. Brook, *Proc. Brit. Ceram. Soc.* **32,** 7 (1982).
16. M. Boudart and S. T. Oyama, *in* "Proceedings, 12th Iberoamerican Symp. Catal., Rio de Janeiro, 1990," p. 793, Brazilian Petroleum Institute.
17. J. S. Lee and S. Locatelli, S. T. Oyama, and M. Boudart, *J. Catal.* **125,** 157 (1990).
18. L. Leclerq, *in* "Surface Properties and Catalysis by Non-Metals" (J. P. Bonenelle, Ed.), Reidel, New York (1983).
19. S. T. Oyama, Ph.D. Dissertation, Stanford University, Stanford, CA (1981).
20. L. Volpe and M. Boudart, *J. Solid State Chem.* **59,** 348 (1985).
21. G. S. Ranhotra, G. W. Haddix, A. T. Bell and J. A. Reimer, *J. Catal.* **108,** 24 (1987).
22. J. S. Lee, S. T. Oyama, and M. Boudart, *J. Catal.* **106,** 125 (1987).
23. J. S. Lee, M. H. Yeom, K. Y. Park, I. S. Nam, J. S. Chung, Y. G. Kim, and S. H. Moon, *J. Catal.* **128,** 126 (1991).
24. L. Volpe and M. Boudart, *J. Solid State Chem.* **59,** 332 (1985).
25. G. Brauer and W. D. Schnell, *J. Less-Common Met.* **6,** 326 (1964).
26. V. A. Epelbaum and A. K. Brager, *Acta Physicochim. URSS* **13,** 595 (1940).
27. D. A. King and F. Sebba, *J. Catal.* **4,** 253 (1965).
28. C. R. Lotz and F. Sebba, *Trans. Faraday Soc.* **53,** 1246 (1957).
29. L. Volpe, Ph.D. Dissertation, Stanford University, Stanford University, CA (1985).
30. S. T. Oyama, J. C. Schlatter, J. E. Metcalf III, J. M. Lambert, Jr., *Ind. Eng. Chem. Res.* **2** 1639 (1988).
31. E. L. Muetterties, "Transition Metal Hydrides," Dekker, New York (1971).
32. K. M. Mackay, "Hydrogen Compounds of the Metallic Elements," Span, London (1966).
33. G. G. Libowitz, "The Solid-State Chemistry of Binary Metal Hydrides," Benjamin, New York 1965.
34. G. Alefeld and J. Volkl (Eds.), "Hydrogen in Metals I, Topics in Applied Physics," Vol. 2 Springer-Verlag, Berlin (1978).
35. Powder Diffraction Data File 31-1439, Inorganic Phases, JCPDS International Center for Diffraction Data, Swathmore, PA (1981).
36. F. S. Galasso, "Structure and Properties of Inorganic Solids," Pergamon, New York (1979).
37. R. J. H. Clark, "The Chemistry of Titanium and Vanadium," Elsevier, New York (1968).
38. N. Schönberg, *Acta. Chem. Scand.* **8,** 221 (1954).
39. B. D. Cullity, "Elements of X-Ray Diffraction, Addison–Wesley, New York (1959).
40. J. M. Smith, "Chemical Engineering Kinetics, 3rd ed., McGraw–Hill, New York (1981).
41. P. J. Anderson and P. L. Morgan, *Trans. Faraday Soc.* **60,** 930 (1964).
42. P. A. Redhead, *Vacuum* **12,** 203 (1962).
43. J. Cvetanovic and Y. Amenomiya, *Catal. Rev.* **6,** 21 (1972).
44. J. L. Falconer and J. A. Schwarz, *Catal. Rev. Sci. Eng.* **25,** 141 (1983).
45. N. W. Hurst, S. J. Gentry, A. Jones, and B. D. McNicol, *Catal. Rev.-Sci. Eng.* **24,** 2 (1982).
46. J. L. Taylor and W. H. Weinberg, *Surf. Sc* **78,** 259 (1978).
47. J. Bruke, "The Kinetics of Phase Transformation in Metals," Pergamon, Oxford (1965).